Energy Materials

Article

Check for updates

Efficient separation and selective Li recycling of spent LiFePO$_4$ cathode

Yuelin Kong, Lixia Yuan[*], Yaqi Liao, Yudi Shao, Shuaipeng Hao, Yunhui Huang[*]

State Key Laboratory of Material Processing and Die and Mold Technology, School of Materials Science and Engineering, Huazhong University of Science and Technology, Wuhan 430074, Hubei, China.

[*]Correspondence to: Prof. Lixia Yuan, State Key Laboratory of Material Processing and Die and Mold Technology, School of Materials Science and Engineering, Huazhong University of Science and Technology, 1037 Luoyu Road, Wuhan 430074, Hubei, China. E-mail: yuanlixia@hust.edu.cn; Prof. Yunhui Huang, State Key Laboratory of Material Processing and Die and Mold Technology, School of Materials Science and Engineering, Huazhong University of Science and Technology, 1037 Luoyu Road, Wuhan 430074, Hubei, China. E-mail: huangyh@hust.edu.cn

Abstract

Given the fast-growing demand for lithium-ion batteries (LIBs) and the upcoming climax of LIB retirement, efficient recycling of spent LIBs has shown increasing importance in both economic benefit and environmental conservation. The LIBs with LiFePO$_4$ (LFP) cathodes account for half of the LIB market, so developing an appropriate recycling way for spent LFP (SLFP) batteries is imperative. In this work, a closed-loop regeneration of SLFP cathodes is proposed, in which a facile cold stimulation route is invented to peel the SLFP layer from Al foil, and then Li and Fe elements are selectively and efficiently extracted from the peeling SLFP layer under mild conditions based on an oxidant of NaClO. The leaching rate of elemental Li could reach 98.3%, and the regenerated LFP synthesized by recovered Li$_2$CO$_3$ and FePO$_4$ shows exceptional performance with a discharge capacity of 162.6 mAh g^{-1} at 0.5 C. This regeneration route has greatly reduced the use of chemical reagents, shortened the process of impurity removal, and, therefore, realized the closed-loop regeneration of SLFP batteries.

Keywords: Spent lithium iron phosphate batteries, cold stimulation, separation, NaClO, selective Li recycling

INTRODUCTION

Since their commercial application in the 1990s, lithium-ion batteries (LIBs) have been widely used in

portable electronics and electric vehicles and in the upcoming blowout era of large-scale electrical energy storage[1-3]. The installed capacity of LIBs has increased from 64.3 GWh in 2017 to 432.7 GWh in 2022 and may exceed 6,500 GWh by 2050[4]. LiFePO$_4$ (LFP), one of the most widely used cathode materials for LIBs, accounts for half of the LIB market. Owing to the strong energy of Fe-O and P-O bonds, the olivine crystal structure of LFP can be well maintained during the repeated lithiation/delithiation cycles, resulting in a long cycle life and good high-temperature stability of the LFP batteries[5,6]. The service life of a LFP battery is generally 5-8 years, and the next few years will be the climax of LFP battery retirement[7]. A large number of spent lithium iron phosphate (SLFP) batteries will soon pose serious environmental and social issues[8]. Therefore, developing an appropriate recycling way for SLFP batteries is a matter of great urgency.

The cathode materials contain Li and other valuable transition-metal elements, accounting for 50% of the cost of LIBs. Therefore, the recycling of spent LIBs mainly concentrates on the recovery and reuse of the cathode materials, which has obvious socioeconomic and environmental benefits[9]. For the SLFP cathode, there are two main recycling routes currently: pyrometallurgy and hydrometallurgy[10,11]. The pyrometallurgy route enriches the precious metal elements or renovates the materials via high temperature treatment[12,13]. As a traditional recovery method, pyrometallurgy is simple to operate and can be adapted to a variety of cathode materials. However, the high temperature process can lead to partial lithium loss, lowering the extraction rate of Li ($< 90\%$)[14]. Moreover, the high-temperature process consumes vast energy and emits large quantities of greenhouse gases, so it is not a sustainable industrial production method[15]. By comparison, hydrometallurgy has advantages of high recovery efficiency, low energy consumption, and limited gas emission[16,17]. But in most of the hydrometallurgy processes, strong inorganic acid or organic acid are usually used to destroy the structure of the cathode materials and extract Li and other valuable metal elements[18-20]. Kumar *et al.* have proposed an organic acid-based leaching strategy to recover SLFP cathodes, in which the leaching rates of Li, Cu, and Al reach 94.83%, 96.92%, and 47.24%, respectively[18]. Ji *et al.* have developed a SLFP recovery method based on the combination of formic acid leaching and hydrogen peroxidation. The leaching rate of Li can reach 98.84%, and the leaching rate of Fe can be less than 1%[21]. However, the strong Fe-O and P-O ionic bonds in the olivine structure hinder the structural destruction and element separation, which makes the effective separation of Li and Fe a challenge in the recovery of SLFP. To solve this problem, oxidants have been proposed as leaching agents[22-24]. Through oxidation, Fe^{2+} in LFP is oxidized to Fe^{3+} as $FePO_4$ precipitation, thus releasing lithium ions, which realize the selective separation of Li and Fe. Peng *et al.* have perfectly implemented the recovery of Li and Fe via a redox reaction between ammonium persulfate and LFP, and Li *et al.* have also separated Li and Fe using hydrogen peroxide[25,26]. Similarly, Yu *et al.* have chosen the $[Fe(CN)_6]^{3-}$ solution as a selective and regenerative redox mediator to break LFP down into $FePO_4$ and Li^+, with a recycling efficiency for Li removal up to 99.8% at room temperature[27]. In addition, there are some novel and valuable recycling methods. Du *et al.* have proposed a strategy to fabricate recyclable-oriented $LiFeMnPO_4$/graphite LIBs with a water-soluble polyacrylic acid binder and carbon paper current collector[28]. Xu *et al.* have proposed a recovery method of roll-to-roll electrodes, using LLZTO membrane to recycle lithium-containing electrodes[29].

Peeling the cathode materials from the Al foil precisely and low-costly has great significance for the following material recovery[30]. At present, two main stripping methods have been used. One is to directly dissolve the Al foil with acid or alkali, realizing the separation of the cathode materials and Al foil[31,32]. The other is to make the binder (polyvinylidene fluoride, PVDF) invalid through heat treatment or organic solvent immersion so that the cathode materials fall off from the Al foil[33,34]. The extensive use of acid, alkali, and organic solvents increases the cost of recovery and also brings serious secondary pollution[35]. More importantly, the content of Al impurities in the cathode materials obtained by these stripping methods is

often high[36]. To achieve high-quality recycling or recovery, a further impurity removal process is required, leading to a longer recovery process and loss of valuable metals.

Herein, a closed-loop regeneration of SLFP cathodes is proposed, in which a facile cold stimulation method is invented to peel the SLFP layer from Al foil, and then Li and Fe are selectively and efficiently extracted from the peelings under mild conditions based on an oxidant of NaClO [Figure 1]. The cold stimulation stripping process does not require any chemical reagents, which controls the cost of reagents and the chemical pollution from the source. Meanwhile, this method effectively reduces the content of Al impurities in the stripped cathode material, which is conducive to the following extract of Li. Furthermore, via the oxidation of NaClO, Fe^{2+} is oxidized to Fe^{3+} as $FePO_4$ precipitation, and Li is extracted from the crystal and converted into soluble lithium salts. A saturated Na_2CO_3 solution is further added to precipitate Li as Li_2CO_3. Finally, the recovered Li_2CO_3 and $FePO_4$ are used as the precursor to obtain LFP. The regenerated LFP (RLFP) demonstrates excellent electrochemical performance, which can deliver a high reversible capacity of 162.6 mAh g^{-1} at 0.5 C and maintain a capacity retention rate of 92.7% after 300 cycles. The closed-loop recovery route achieves a leaching rate of 98.3% for Li, which provides a potential route for the recycling of the SLFP cathode.

EXPERIMENTAL SECTION
Materials and reagents
The SLFP batteries were obtained from Guangzhou Energy Very Endure Co., Ltd, China. NaClO solution (Available chlorine 12%), Na_2CO_3, HCl, NaOH, and sucrose were purchased from Aladdin Reagent Co., Ltd (Shanghai, China). All the chemical reagents used in this work were of analytical grade.

Experimental procedures
Stripping of SLFP cathodes
After discharging below 3.0 V, the SLFP batteries were disassembled in the glove box. The obtained SLFP cathode sheets were cut into small pieces with 1 cm. The small pieces were put into a 25 mL beaker with 5 mL deionized water added. Then, the beaker was put into the refrigerator to freeze until the water was completely frozen. The frozen beaker was transferred into the freezer dryer for drying. During the drying process, the SLFP layer was stripped from the Al foil completely, and no external force was required. The content of Li, P, Fe, and Al in the stripped SLFP layer was measured by an inductively coupled plasma-optical emission spectrometer (ICP-OES).

Selective leaching of Li and Fe
All leaching experiments were carried out in a 500 mL beaker, with a magnetic stirrer heating and stirring. Firstly, a 5 g stripped SLFP layer was mixed with deionized water in the beaker with different solid-liquid ratios. Then, a certain volume of NaClO solution (pH = 11) was added. The pH of the reaction system was adjusted with a small amount of hydrochloric acid, and the oxidation leaching reaction was conducted at magnetic stirring of 300 r min^{-1}. In this process, Li was selectively leached into the solution, and Fe^{2+} was oxidized to Fe^{3+} as $FePO_4$ precipitation. At the same time, due to the oxidation of NaClO, the PVDF binder failed, and conductive carbon was released. Low-density conductive carbon floated on the upper layer of the solution, which was collected first. Then, via vacuum filtration, Li^+ solution and $FePO_4$ precipitation were obtained. The $FePO_4$ precipitation was washed with deionized water three times and was used as a precursor for RLFP after drying. The pH of the Li^+ solution was adjusted to 13 with NaOH solution, and then saturated Na_2CO_3 solution was added to obtain white Li_2CO_3 precipitation after heating and boiling for 30 min. The Li_2CO_3 precipitation was washed with boiling water three times and dried at 90 °C for 12 h, which was directly used as a Li source for the RLFP.
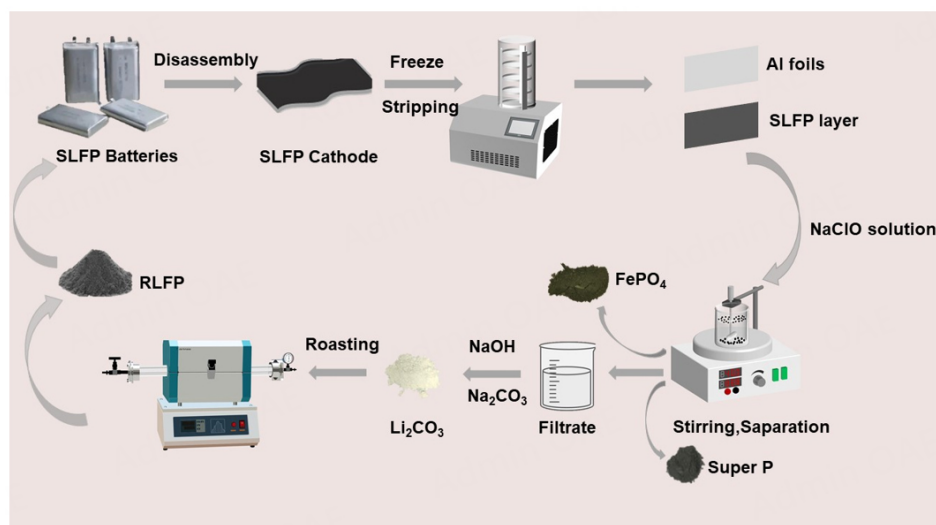
Figure 1. Schematic illustration of the recycling route for the SLFP cathode.

In order to optimize the leaching conditions, the reaction time (0.5-3.0 h), temperature (20-40 °C), system pH (1-9), solid-liquid ratio (10-100 g L^{-1}), and NaClO dosage (NaClO:SLFP = 0.85:1.05) were systematically investigated. After the leaching reaction, the content of Li, P, Fe, and Al in the solution was measured by ICP-OES. The leaching efficiency of each element is calculated using the formula reported in the literature:

$$R = \frac{C \times V}{m \times \omega\%}$$

where R represents the leaching rate of the target element (%), C represents the concentration of the target element in the solution (g L^{-1}), V represents the volume of the solution (V), m represents the mass of the stripped cathode materials participating in the reaction (g), and ω% represents the mass proportion of the target element in the stripped cathode materials[37].

Regeneration of LiFePO$_4$

The recovered Li_2CO_3 and $FePO_4$ were mixed at a molar ratio of 1.05:1, and 10 wt% sucrose was added as the carbon source. Ethanol was added as a dispersant, and the mixture was ball milled for 5 h at a speed of 400 r min^{-1}. Then, the precursor powder was dried at 70 °C for 3 h. The dried powder was put into a muffle furnace for roasting. In the argon atmosphere, the temperature was firstly raised to 350 °C at the rate of 5 °C min^{-1} and kept for 2 h, and then the heating temperature was continued up to 750 °C and maintained for 4 h. After cooling to room temperature, the RLFP powder was obtained.

Characterization

The morphology and crystal structure were observed on Quanta650 FEG scanning electron microscope (FEI, America) and JEM-F200 HR-TEM (JEOL, Japan). X-ray diffraction (XRD) patterns were analyzed by XRD-6100 (Shimadzu, Japan). Fourier-transform infrared (FT-IR) spectrum was conducted by a Spectrum one FT-IR spectrophotometer (Thermo Scientific Nicolet iS20, America). X-ray photoelectron spectroscopy (XPS) was performed with an AXIS-ULTRA DLD-600W spectrometer (Kratos, Japan). The concentration of elements was analyzed by Agilent 730 ICP-OES (PerkinElmer, America).

The regenerated cathodes were made by mixing the RLFP powder, PVDF binder, and super P in a ratio of 9:0.5:0.5 with N-methyl pyrrolidone (NMP) as the solvent to get slurry. Then, the mixed slurry was uniformly coated on the Al foil and dried at 100 °C for 12 h. The half-cells were assembled with the RLFP cathode, lithium metal anode, and electrolyte in an Ar-filled glove box. The electrolyte was 1 M LiPF$_6$ in an equal mixture of ethyl carbonate (EC) and diethyl carbonate (DEC). The relative electrochemical performances, such as rate capability and cycling stability, of RLFP and SLFP were recorded in a voltage window of 2.5-4.2 V using a Land battery test system (MIHW-200-160CH). Cyclic voltammetry (CV) and electrochemical impedance spectroscopy (EIS) were performed using an electrochemical workstation (DH 7000, Donghua Testing Technology Co., Ltd).

RESULTS AND DISCUSSION
Stripping of SLFP cathodes
The closed-loop regeneration route based on the cold stimulation peeling and NaClO oxidative extraction is illustrated in Figure 1 and Supplementary Figure 1. The strong adhesive strength of PVDF makes it difficult to separate Al and cathode materials completely. The traditional reagent dissolution method is expensive and may bring high content Al impurities in the stripped cathode materials. Here, the cold stimulation route is cheap and environmentally friendly. Figure 2A and E shows images of the untreated SLFP cathode, and Figure 2C shows the section. It can be seen that the cathode material is closely connected to the Al foil, and the electrode surface is dense and uniform. During the freeze-drying process, the SLFP layer is separated from the Al foil [Supplementary Figure 2A]. The glass transition temperature of PVDF ranges from -20 °C to -40 °C so that the long chains of PVDF will break and fail during the freeze-drying process[38]. The SEM images in Figure 2D and F show that the cathode layer separates with the Al foil, and the stripped layer becomes loose and porous. As shown in Figure 2B, the Al foil, after the cold stimulation stripping, is clean and smooth. Supplementary Figure 2C and D compares the SEM images of recycled Al foil and commercial Al foil. Obviously, there is no corrosion on the surface of the recovered Al foil. The XRD spectra in Supplementary Figure 2B show the diffraction peaks of the recovered Al foil agree well with those of the commercial Al foil [Supplementary Figure 2B]. The ICP-OES result shows that the Al impurity content is only 0.03% in the stripped SLFP cathode layer, which could be ignored [Supplementary Table 1]. Obviously, the cold stimulation route controls the Al impurity from the source, which simplifies the post processing efficiently.

Leaching mechanism
As a cheap oxidant, NaClO is widely used as a bleaching agent in the industries of daily-use chemicals, papermaking, and water treatment. In this work, it was selected to leach the peeling SLFP layer via an oxidizing way. Without NaClO addition, the peeling SLFP layer was treated with ultrapure water under the same reaction conditions for comparison. No change can be observed, and no Li and Fe can be detected in the leaching solution [Supplementary Table 2]. As NaClO is added, a black granular floating substance rises. The XRD analysis shows that the floating mixture is mainly C [Supplementary Figure 3A]. Via ICP-OES analysis, the Li content in the leaching solution is identified as 1,062.48 mg L^{-1}, and the Fe content is 3.06 mg L^{-1}. Obviously, NaClO can invalidate PVDF, so SLFP and the conductive carbon are released. The light carbon and PVDF residue float to the upper layer of the mixture. The failure mechanism of PVDF is analyzed. From the FT-IR spectrum in Supplementary Figure 3B and C, it can be seen that after being treated with NaClO, the pure PVDF and the SLFP layer both present obvious hydroxyl and carbonyl peaks, indicating that NaClO could oxidize PVDF and, therefore, invalidate the adhesion. To sum up, the main ionic reaction occurs according to the following reaction equation in this system:

$$ClO^- + 2H^+ + 2LiFePO_4 = 2FePO_4 + 2Li^+ + H_2O + Cl^-.$$
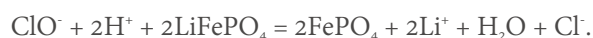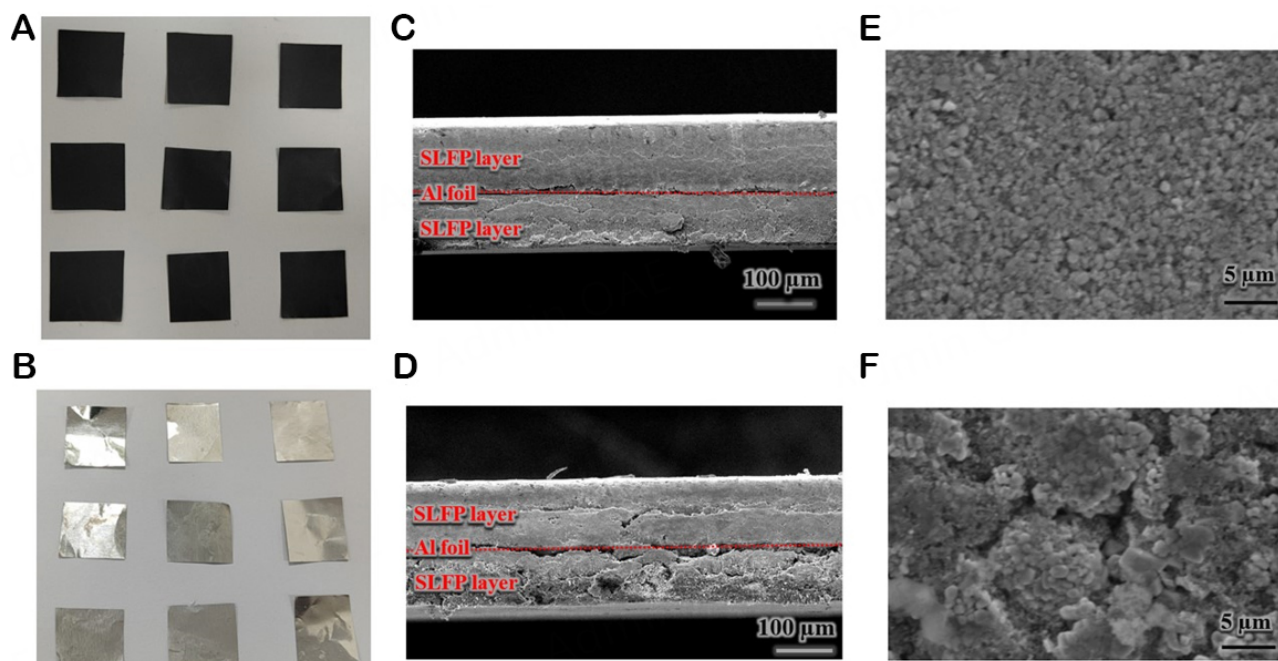
Figure 2. (A and B) digital photos of SLFP cathodes and Al foil. (C and D) Cross-section SEM images of SLFP cathodes and SLFP cathodes after freeze drying. (E and F) SEM images of SLFP cathodes and peeling SLFP layers.

By adding saturated Na_2CO_3 solution into the Li leaching solution, white Li_2CO_3 powder is obtained, identified by XRD analysis [Figure 3A]. The SEM images in Figure 3B demonstrate that the obtained Li_2CO_3 has a rod-like structure. The solid precipitate at the bottom is orthogonal $FePO_4$ (JCPDS: 37-0478, Figure 3C), which has no impurity. The SEM and element mapping analysis [Figure 3D-F] show the $FePO_4$ particles are uniform, and the P, Fe, and O elements are evenly distributed. The regenerated $FePO_4$ is directly used as the precursor for the following RLFP preparation.

Optimization of leaching conditions

The dosage of NaClO, reaction temperature, reaction time, pH of the system, and solid-liquid ratios were systematically optimized. Figure 4A shows the leaching efficiency of each element at different NaClO dosages. When the molar ratio of NaClO to SLFP reaches 1:1, the leaching rate of Li is up to 98.3%, and the leaching rate of iron can be ignored, indicating that the selective separation of Li and Fe has been achieved. The leaching efficiency of Li declines when the molar ratio of NaClO to SLFP reaches 1.05:1. This is due to the decomposition of NaClO at higher concentrations. From Figure 4B, it can be seen the leaching rate of Li reaches its highest at 30 °C and declines as temperature further increases. The latter drop can be ascribed to the accelerated decomposition rate of NaClO, which results in an incomplete leaching reaction. Figure 4C shows that Li reaches saturation in the solution after 2 h. Figure 4D shows the leaching rate increases with the decrease of pH. However, strong acidity leads to the dissolving of $FePO_4$. Therefore, the pH of the system is controlled at 2 finally. At last, the solid-liquid ratio is evaluated from 10 g L^{-1} to 100 g L^{-1}. As shown in Figure 4E, the optimal solid-liquid ratio is 50 g L^{-1}. After optimization, the leaching rate of Li reaches 98.3%; the leaching rate of Fe is only 0.11%, and the Al content in the solution is nearly 0%. So, the overall leaching efficiencies of both Fe and Al are low, which has little impact on the final Li extraction.
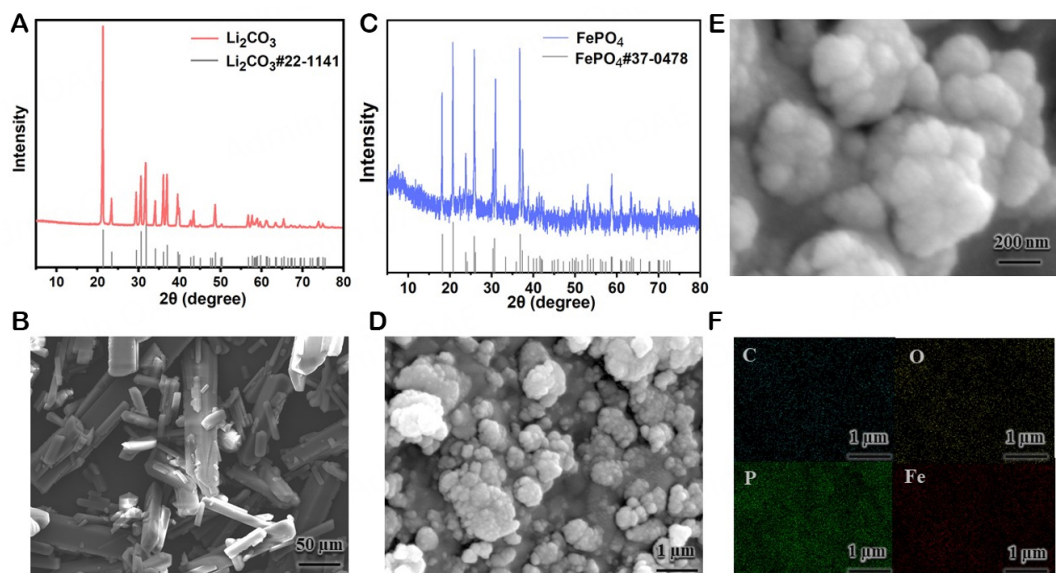
Figure 3. (A and B) XRD characterization patterns and SEM images of recycled Li_2CO_3. (C) XRD characterization patterns of recycled $FePO_4$. (D and E) SEM images of recycled $FePO_4$. (F) EDS mapping of recycled $FePO_4$ [corresponding to (D)].
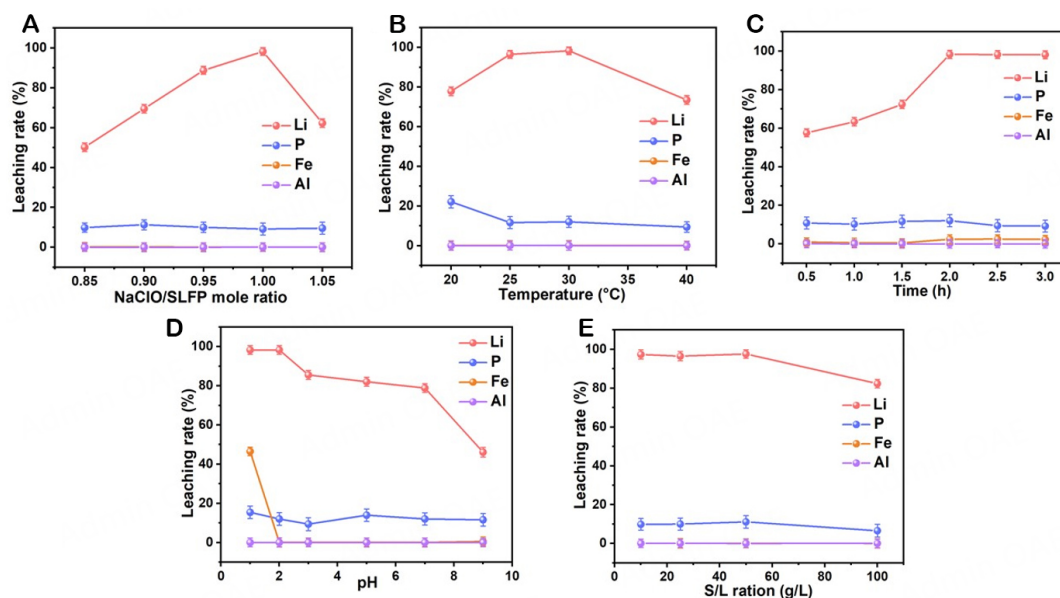
Figure 4. The effects of (A) the mole ratio of NaClO and SLFP, (B) reaction temperature, (C) reaction time, (D) pH of the system, and (E) S/L ratio on leaching efficiencies of Li, P, Fe, and Al.

Kinetics analysis

To grasp the characteristics of the NaClO reactions, the kinetic model was evaluated. The oxidation reaction is considered as the rate control step in the whole leaching process. The formation of $FePO_4$ layers in the oxidation process conforms to the typical shrinking core model, including external diffusion, internal diffusion, and chemical reaction[39]. Under certain conditions, they can act as a control step of the leaching reaction respectively. Based on the optimal leaching condition, the relations of the Li leaching efficiency with reaction temperatures (20 °C, 25 °C, 30 °C, 40 °C) and time (0-3 h) were recorded. Detailed descriptions and data were provided in Supplementary Text 1 and Supplementary Tables 3-6. As mentioned

in Figure 5A, with temperature increasing, the leaching efficiency of Li rises at first and then falls. To determine the rate control step, kinetics fitting for external diffusion, internal diffusion, and chemical reaction is performed according to the corresponding kinetic equations [Supplementary Table 7]. Figure 5B shows the linear correlation coefficient R^2 of internal diffusion is 0.999 at 30 °C, which is much higher than the linear correlation coefficient R^2 (0.966) of external diffusion and the linear correlation coefficient R^2 (0.980) of a chemical reaction. Similarly, at other temperatures, the R^2 of internal diffusion [Figure 5C] is also the highest one among the steps [Supplementary Figure 4]. Therefore, it can be speculated that the internal diffusion process of the oxidant is more critical than the other two steps, which is the control step during the whole leaching reaction. According to the Arrhenius equation [Supplementary Text 2], the relationship between ln k and 1000/T is shown in Figure 5D, and the correlation coefficient is high (R^2 = 0.989). Based on the slope, the apparent activation energy is calculated as 14.55 kJ mol^{-1}.

Regeneration of LiFePO$_4$
The recovered Li_2CO_3 and $FePO_4$ were used to synthesize RLFP directly. Figure 6A and B shows the morphology of the obtained RLFP. Compared with the commercial LFP (CLFP) [Supplementary Figure 5A and B], both the RLFP and CLFP particles distribute loosely. From the results of particle size distribution, the diameter of the RLFP grains is 0.91 ± 0.15 µm, and the size distribution is uniform [Supplementary Figure 6A], which is consistent with the CLFP (0.98 ± 0.14 µm) [Supplementary Figure 6B]. The element mapping in Figure 6C and Supplementary Figure 5C shows that Fe, P, O, and C are evenly distributed in RLFP and CLFP. Figure 6D shows the HRTEM image of the RLFP. A uniform carbon layer (4 nm) is clearly observed on the RLFP particles. Via the HRTEM observation [Figure 6D and Supplementary Figure 5D], regular lattice stripes can be identified inside the RLFP and CLFP, of 4.26 Å and 4.19 Å, corresponding to the (101) crystal plane of LFP. The XRD curves of RLFP and SLFP in Figure 6E show that the peak strength of RLFP is significantly higher than that of SLFP, implying the improved crystallinity of SLFP. The characteristic peaks of RLFP mainly appear at 20.79°, 25.58°, 29.69°, and 35.62°, corresponding to (101), (111), (211), and (311) planes, respectively, which are highly consistent with the standard LFP (PDF 81-1173). No impurity can be detected. Figure 6F compares the Fe 2p spectrum of SLFP and RLFP. Two obvious peak shifts are observed in both materials, while the Fe $2p_{3/2}$ peak moves from 712.4 eV to 710.3 eV, and the Fe $2p_{1/2}$ peak moves from 725.3 eV to 724.5 eV for RLFP, indicating that SLFP (Fe^{3+}) changes to RLFP (Fe^{2+}) completely.

Electrochemical performances
The electrochemical performances of SLFP and RLFP were compared. Figure 7A shows the CV curves of RLFP and SLFP from 2.5 to 4.2 V at a scanning rate of 0.1 mV s^{-1}. The cathodic and anodic peaks of RLFP are 3.58 V and 3.29 V, respectively, corresponding to the Fe^{2+}/Fe^{3+} redox reaction. The potential intervals of RLFP (0.29 V) are much smaller than that of SLFP (0.48 V), and the peak intensity of RLFP is higher, indicating that RLFP has smaller polarization and better electrochemical activity. The charge/discharge voltage plateau gap of RLFP in Figure 7B is narrower than that of SLFP, which agrees well with the CV result. The initial reversible specific capacity of RLFP is 162.6 mAh g^{-1}, much higher than that of SLFP (133.6 mAh g^{-1}) at 0.5 C. Figure 7C shows the rate performance of RLFP at different current densities. It can deliver capacities of 166.1 mAh g^{-1}, 162.6 mAh g^{-1}, 154.3 mAh g^{-1}, 140.4 mAh g^{-1}, and 120.6 mAh g^{-1} at 0.2 C, 0.5 C, 1 C, 2 C, and 5 C, respectively. When the charge/discharge rate returns to 0.5 C again, the discharge specific capacity of RLFP recovers [Figure 7D]. It is worth noting that the specific discharge capacity of RLFP remains at 73.1% even at 5 C, compared with that of 0.2 C. In contrast, the discharge capacity of SLFP demonstrates only 73.5 mAh g^{-1} at 5 C, corresponding to 54.6% of that at 0.2 C. It can be seen the reversible capacity and cycle stability of RLFP are comparable to the CLFP in Figure 7E. The initial discharge capacity and the capacity retention (after 300 cycles) of RLFP are 162.6 mAh g^{-1} (0.5 C) and 92.7%, respectively, which are quite close to those of the CLFP (167.5 mAh g^{-1} and 90.3%). At the same time, the Coulombic
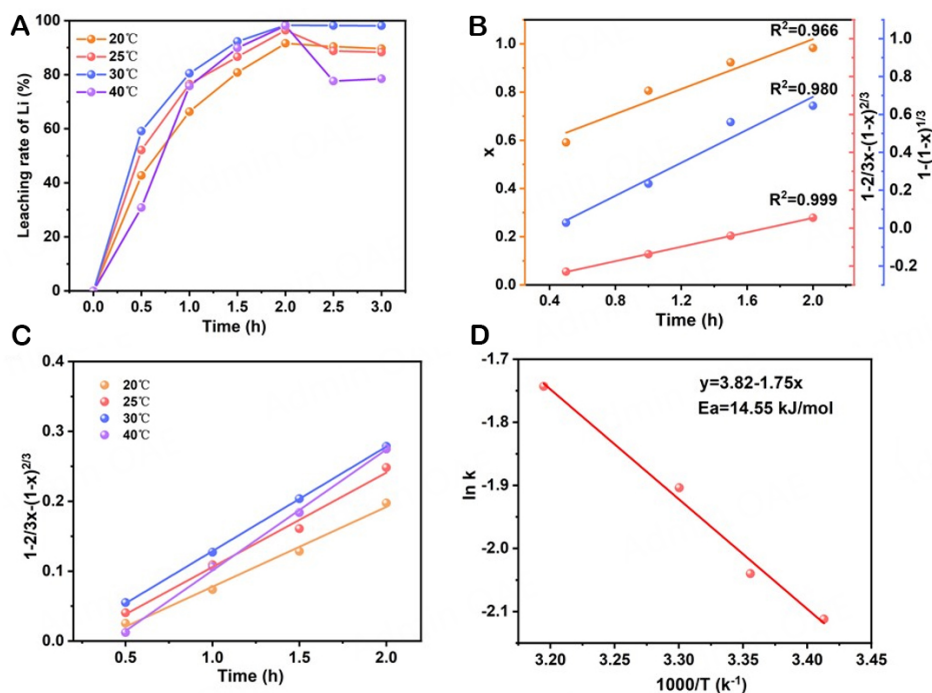
Figure 5. (A) The leaching efficiency of Li^+ at different temperatures varies with time. (B) Kinetics fitting diagram of different leaching models at 30 °C. (C) Kinetics fitting result of internal diffusion at different temperatures varies with time. (D) Arrhenius diagram of ln k-1000/T based on the rate control step.
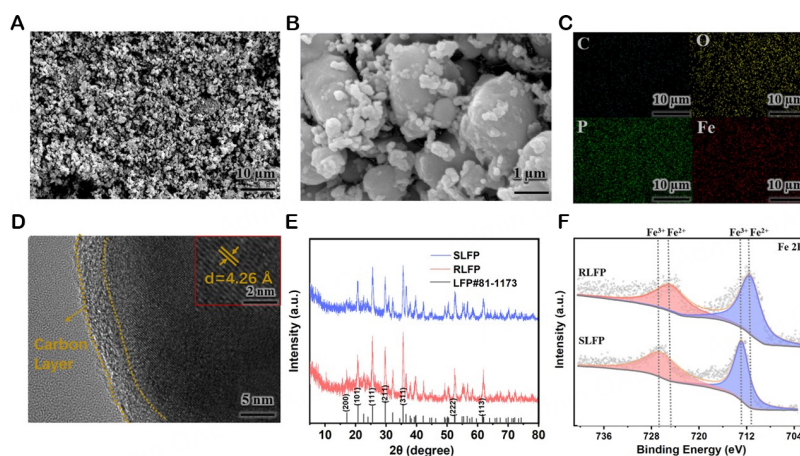
Figure 6. (A and B) SEM images of RLFP. (C) EDS mapping of RLFP [corresponding to (A)] (D) HRTEM images of RLFP nanoparticles. (E) XRD characterization patterns of SLFP and RLFP. (F) XPS spectra of Fe 2p in RLFP and SLFP.

Efficiency of RLFP remains stable above 99.8% throughout the cycles. In contrast, the SLFP shows a low discharge capacity of 133.6 mAh g^{-1} at 0.5 C, with a dramatic capacity decline after 200 cycles.

The lithium-ion diffusion coefficients (D_{Li}^+) of RLFP and SLFP were analyzed by an EIS test. The Nyquist plots are shown in Supplementary Figure 7A, in which the semi-circle indicates the charge transfer resistance (R_{ct}), and the straight line relates to the Li^+ diffusion process. Obviously, the R_{ct} of the RLFP (66.2 Ω) is significantly decreased compared with that of SLFP (499.9 Ω). D_{Li}^+ is calculated according to the inclined line in the lower frequency [Supplementary Figure 7B]. The detailed formula and calculation
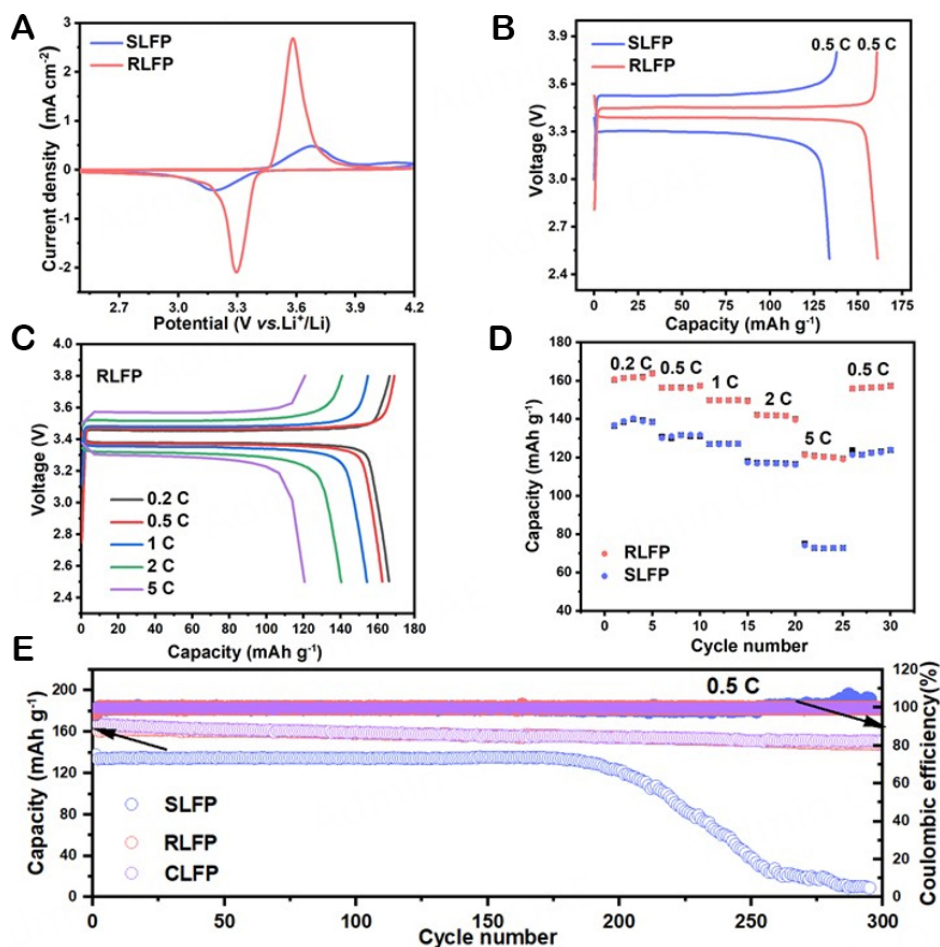
Figure 7. (A) Cyclic voltammetry and (B) the initial charge/discharge curves of SLFP and RLFP. (C) The charge/discharge profiles for RLFP at different rates. (D) Rate performance and (E) long-term cycling stability at 0.5 C for 300 cycles of SLFP, RLFP, and CLFP.

process are listed in Supplementary Text 3 and Supplementary Table 8. The calculation results show that the Li^+ diffusion of RLFP (1.62×10^{-15} cm^2 s^{-1}) is obviously higher than that of SLFP (9.98×10^{-16} cm^2 s^{-1}), implying better electron/ion transportation rate and reaction kinetics.

CONCLUSIONS

In summary, the closed-loop regeneration route based on the cold stimulation peeling combined with NaClO oxidation separation has three clear advantages. Firstly, the overall process does not involve much strong acid or base, so it is quite environmentally friendly. Secondly, the simple cold stimulation process realizes a negligible Al impurity in the stripped cathode material, which greatly simplifies the subsequent impurity removal process. Finally, the oxidation process based on NaClO realizes the selective separation of Li and Fe efficiently. The leaching rate of Li could reach 98.3%, and the RLFP synthesized by recovered Li_2CO_3 and $FePO_4$ has exceptional performance with a discharge capacity of 162.6 mAh g^{-1} along with a capacity retention of 92.7% after 300 cycles (0.5 C). The efficient closed-loop regeneration route provides an innovative approach for the sustainable development of SLFP batteries.

DECLARATIONS

Authors' contributions
Methodology, investigation, and writing manuscript: Kong Y
Project administration and funding acquisition: Yuan L
Analyzed the data: Liao Y
Discussed the whole paper: Shao Y
Performed the measurements: Hao S
Conceptualization and supervision: Huang Y

Availability of data and materials
The data supporting our work can be found in the Supplementary Materials.

Financial support and sponsorship
This work was supported by the National Natural Science Foundation of China (Grant No. 22075091) and the Natural Science Foundation of Hubei Province (Grant No. 2021CFA066).

Conflicts of interest
All authors declared that there are no conflicts of interest.

Ethical approval and consent to participate
Not applicable.

Consent for publication
Not applicable.

Copyright
© The Author(s) 2023.

REFERENCES

1. Liu H, Strobridge FC, Borkiewicz OJ, et al. Capturing metastable structures during high-rate cycling of LiFePO$_4$ nanoparticle electrodes. *Science* 2014;344:1252817. DOI
2. Yan Y, Zeng T, Liu S, Shu CZ, Zeng Y. Lithium metal stabilization for next-generation lithium-based batteries: from fundamental chemistry to advanced characterization and effective protection. *Energy Mater* 2023;3:300002. DOI
3. Wu F, Maier J, Yu Y. Guidelines and trends for next-generation rechargeable lithium and lithium-ion batteries. *Chem Soc Rev* 2020;49:1569-614. DOI PubMed
4. Miao Y, Liu L, Zhang Y, Tan Q, Li J. An overview of global power lithium-ion batteries and associated critical metal recycling. *J Hazard Mater* 2022;425:127900. DOI
5. Fan MC, Zhao Y, Kang YQ, et al. Room-temperature extraction of individual elements from charged spent LiFePO$_4$ batteries. *Rare Met* 2022;41:1595-604. DOI
6. Zhang B, He Y, Gao H, et al. Unraveling the doping mechanisms in lithium iron phosphate. *Energy Mater* 2022;2:200013. DOI
7. Ciez RE, Whitacre JF. Examining different recycling processes for lithium-ion batteries. *Nat Sustain* 2019;2:148-56. DOI
8. Nanda S, Berruti F. Municipal solid waste management and landfilling technologies: a review. *Environ Chem Lett* 2021;19:1433-56. DOI
9. Gangaja B, Nair S, Santhanagopalan D. Reuse, recycle, and regeneration of LiFePO$_4$ cathode from spent lithium-ion batteries for rechargeable lithium- and sodium-ion batteries. *ACS Sustain Chem Eng* 2021;9:4711-21. DOI
10. Song X, Hu T, Liang C, et al. Direct regeneration of cathode materials from spent lithium iron phosphate batteries using a solid phase sintering method. *RSC Adv* 2017;7:4783-90. DOI
11. Zhao Y, Yuan X, Jiang L, et al. Regeneration and reutilization of cathode materials from spent lithium-ion batteries. *Chem Eng J* 2020;383:123089. DOI
12. Makuza B, Tian Q, Guo X, Chattopadhyay K, Yu D. Pyrometallurgical options for recycling spent lithium-ion batteries: a comprehensive review. *J Power Sources* 2021;491:229622. DOI
13. Holzer A, Windisch-kern S, Ponak C, Raupenstrauch H. A novel pyrometallurgical recycling process for lithium-ion batteries and its application to the recycling of LCO and LFP. *Metals* 2021;11:149. DOI

14. Liu F, Peng C, Porvali A, Wang Z, Wilson BP, Lundström M. Synergistic recovery of valuable metals from spent nickel-metal hydride batteries and lithium-ion batteries. *ACS Sustain Chem Eng* 2019;7:16103-11. DOI

15. Jin S, Mu D, Lu Z, et al. A comprehensive review on the recycling of spent lithium-ion batteries: urgent status and technology advances. *J Clean Prod* 2022;340:130535. DOI

16. Yao Y, Zhu M, Zhao Z, Tong B, Fan Y, Hua Z. Hydrometallurgical processes for recycling spent lithium-ion batteries: a critical review. *ACS Sustain Chem Eng* 2018;6:13611-27. DOI

17. Jung JC, Sui P, Zhang J. A review of recycling spent lithium-ion battery cathode materials using hydrometallurgical treatments. *J Energy Stor* 2021;35:102217. DOI

18. Kumar J, Shen X, Li B, Liu H, Zhao J. Selective recovery of Li and $FePO_4$ from spent $LiFePO_4$ cathode scraps by organic acids and the properties of the regenerated $LiFePO_4$. *Waste Manag* 2020;113:32-40. DOI

19. Yue XH, Zhang CC, Zhang WB, Wang Y, Zhang FS. Recycling phosphorus from spent $LiFePO_4$ battery for multifunctional slow-release fertilizer preparation and simultaneous recovery of Lithium. *Chem Eng J* 2021;426:131311. DOI

20. Qiu HJ, Hao XD, Gui YX, Liu XT, Chen G, Gao L. Recent progresses in recycling technology for cathode materials from spent lithium iron phosphate batteries. *Modern Chem Ind* 2022;42:60-4, 69. DOI

21. Ji G, Ou X, Zhao R, et al. Efficient utilization of scrapped $LiFePO_4$ battery for novel synthesis of $Fe_2P_2O_7$/C as candidate anode materials. *Resour Conserv Recycl* 2021;174:105802. DOI

22. He K, Zhang ZY, Zhang FS. A green process for phosphorus recovery from spent $LiFePO_4$ batteries by transformation of delithiated $LiFePO_4$ crystal into $NaFeS_2$. *J Hazard Mater* 2020;395:122614. DOI

23. Dai Y, Xu Z, Hua D, Gu H, Wang N. Theoretical-molar Fe^{3+} recovering lithium from spent $LiFePO_4$ batteries: an acid-free, efficient, and selective process. *J Hazard Mater* 2020;396:122707. DOI

24. Yang Y, Zheng X, Cao H, et al. A closed-loop process for selective metal recovery from spent lithium iron phosphate batteries through mechanochemical activation. *ACS Sustain Chem Eng* 2017;5:9972-80. DOI

25. Peng D, Zhang J, Zou J, et al. Closed-loop regeneration of $LiFePO_4$ from spent lithium-ion batteries: a "feed three birds with one scone" strategy toward advanced cathode materials. *J Clean Prod* 2021;316:128098. DOI

26. Li H, Xing S, Liu Y, Li F, Guo H, Kuang G. Recovery of lithium, iron, and phosphorus from spent $LiFePO_4$ batteries using stoichiometric sulfuric acid leaching system. *ACS Sustain Chem Eng* 2017;5:8017-24. DOI

27. Yu J, Wang X, Zhou M, Wang Q. A redox targeting-based material recycling strategy for spent lithium ion batteries. *Energy Environ Sci* 2019;12:2672-7. DOI

28. Du H, Kang Y, Li C, et al. Easily recyclable lithium-ion batteries: recycling-oriented cathode design using highly soluble $LiFeMnPO_4$ with a water-soluble binder. *Battery Energy* 2023;2:20230011. DOI

29. Xu J, Jin Y, Liu K, et al. A green and sustainable strategy toward lithium resources recycling from spent batteries. *Sci Adv* 2022;8:eabq7948. DOI PubMed PMC

30. Liu H, Zhang JL, Liang GQ, Wang M, Chen YQ, Wang CY. Selective lithium recovery from black powder of spent lithium-ion batteries via sulfation reaction: phase conversion and impurities influence. *Rare Met* 2023;42:2350-60. DOI

31. Fan E, Li L, Wang Z, et al. Sustainable recycling technology for Li-ion batteries and beyond: challenges and future prospects. *Chem Rev* 2020;120:7020-63. DOI

32. Li L, Fan E, Guan Y, et al. Sustainable recovery of cathode materials from spent lithium-ion batteries using lactic acid leaching system. *ACS Sustain Chem Eng* 2017;5:5224-33. DOI

33. Jing Q, Zhang J, Liu Y, Zhang W, Chen Y, Wang C. Direct regeneration of spent $LiFePO_4$ cathode material by a green and efficient one-step hydrothermal method. *ACS Sustain Chem Eng* 2020;8:17622-8. DOI

34. Liu K, Zhang FS. Innovative leaching of cobalt and lithium from spent lithium-ion batteries and simultaneous dechlorination of polyvinyl chloride in subcritical water. *J Hazard Mater* 2016;316:19-25. DOI

35. Ji Y, Jafvert CT, Zyaykina NN, Zhao F. Decomposition of PVDF to delaminate cathode materials from end-of-life lithium-ion battery cathodes. *J Clean Prod* 2022;367:133112. DOI

36. Widijatmoko SD, Fu G, Wang Z, Hall P. Recovering lithium cobalt oxide, aluminium, and copper from spent lithium-ion battery via attrition scrubbing. *J Clean Prod* 2020;260:120869. DOI

37. Xu Y, Qiu X, Zhang B, et al. Start from the source: direct treatment of a degraded $LiFePO_4$ cathode for efficient recycling of spent lithium-ion batteries. *Green Chem* 2022;24:7448-57. DOI

38. Hronsk V, Jozef M. Thermally stimulated depolarization and mechanical relaxation study of glass transition in polyvinylidene fluoride. *Acta Phys Slovaca* 2002;52:91-100. Available from: https://www.researchgate.net/publication/256086873 [Last accessed on 8 Nov 2023]

39. Li L, Bian Y, Zhang X, et al. Process for recycling mixed-cathode materials from spent lithium-ion batteries and kinetics of leaching. *Waste Manag* 2018;71:362-71. DOI